IOP Publishing Nanotechnology
Nanotechnology **25** (2014) 385602 (13pp) doi:10.1088/0957-4484/25/38/385602

Vacancy formation on C60/Pt (111): unraveling the complex atomistic mechanism

Anna L Pinardi[1], Giulio Biddau[2], Kees van De Ruit[3], Gonzalo Otero-Irurueta[1,6], Sara Gardonio[4], Silvano Lizzit[4], Robert Schennach[5], Cees F J Flipse[3], María F López[1], Javier Méndez[1], Rubén Pérez[2,7] and José A Martín-Gago[1]

[1] ESISNA Group Instituto de Ciencia de Materiales de Madrid (CSIC), c/ Sor Juana Inés de la Cruz, E-28049 Madrid, Spain
[2] Departamento de Física Teórica de la Materia Condensada, Universidad Autónoma de Madrid, E-28049 Madrid, Spain
[3] Molecular Materials and Nanosystems, Eindhoven University of Technology, 5600 MB, Eindhoven, The Netherlands
[4] Sincrotrone Trieste S.C.p.A, Strada Statale 14, Km. 163.5, I-34149 Trieste, Italy
[5] Institute of Solid State Physics, Graz University of Technology, Graz, Austria
[6] Center for Mechanical Technology & Automation-TEMA, University of Aveiro, 3810-193 Aveiro, Portugal
[7] Condensed Matter Physics Center (IFIMAC), Universidad Autónoma de Madrid, E-28049-Madrid, Spain

E-mail: gago@icmm.csic.es and Ruben.perez@uam.es

Received 12 June 2014, revised 25 July 2014
Accepted for publication 30 July 2014
Published 2 September 2014

Abstract

The interaction of fullerenes with transition metal surfaces leads to the development of an atomic network of ordered vacancies on the metal. However, the structure and formation mechanism of this intricate surface reconstruction is not yet understood at an atomic level. We combine scanning tunneling microscopy, high resolution and temperature programmed-x-ray photoelectrons spectroscopy, and density functional theory calculations to show that the vacancy formation in C60/Pt(111) is a complex process in which fullerenes undergo two significant structural rearrangements upon thermal annealing. At first, the molecules are physisorbed on the surface; next, they chemisorb inducing the formation of an adatom–vacancy pair on the side of the fullerene. Finally, this metastable state relaxes when the adatom migrates away and the vacancy moves under the molecule. The evolution from a weakly-bound fullerene to a chemisorbed state with a vacancy underneath could be triggered by residual H atoms on the surface which prevent a strong surface-adsorbate bonding right after deposition. Upon annealing at about 440 K, when all H has desorbed, the C60 interacts with the Pt surface atoms forming the vacancy-adatom pair. This metastable state induces a small charge transfer and precedes the final adsorption structure.

Keywords: STM, DFT, fullerene, vacancy network, molecular structure

(Some figures may appear in colour only in the online journal)

1. Introduction

Fullerenes are one of the most amazing molecules in nanoscience. Fullerenes combined in dyads with other organic molecules are efficient organic photovoltaic materials [1, 2], and this has recently stimulated their research in the form of thin films. Moreover, C_{60} is a special molecule due to its large stability and its spherical shape, and it is considered a

model system to address many fundamental questions about the interaction of cyclic-organic molecules with surfaces.

C_{60} usually forms large-unit-cell self-assembled monolayers when deposited on metal surfaces [3]. There is an extended bibliography on thin films of C_{60} on many different single crystal metal substrates as Pt [4–10], Al [11, 12], Cu [13–18], Au [19–28] and Ag [29–34] or even on graphene [35], among many others. On some metals, when deposited at room temperature (RT), C_{60} interacts with both the metallic surface and the surrounding molecules by van der Waals (vdW) interactions. In this case, the molecules usually form weakly assembled close-packed layers separated by the vdW radius, which slightly adjusts to match the substrate symmetry. However, on some other metallic surfaces, and especially after annealing, C_{60} has been found to generate nanopatterning on the surface by a surface-adsorbate covalent bond. In particular, it has been surprisingly shown that fullerenes induce nano-pits at an atomic level on some surfaces, like Pt(111). Felici *et al* [4] in 2005 published the first experimental observation of the formation of an ordered network of atomic vacancies in a surface caused by the presence of fullerenes. Using surface x-ray diffraction, they found out that one atom below each C_{60} was removed on Pt (111) upon annealing. This result set a trend of experiments on similar systems where a single- or a multi-atom vacancy has been observed. Indeed, the presence of vacancies in C_{60}/metal systems have also been reported on many metals such as Au(111), Au(110), Ag(111), Cu(111), Al(111) and Pt(110) [11, 13, 15, 20, 21, 24, 28, 36–39]. Thus, single-atom vacancy formation has been suggested to be 'the rule rather than the exception' [36].

Most of the abovementioned works use scanning tunneling microscopy (STM) to infer the orientation of the molecule with respect to the surface by resolving the empty molecular orbitals (MO) [26]. On a C_{60} molecule the largest electron density is confined in the pentagons of the fullerene cage [26]. Thus, if for example the C_{60} molecules are adsorbed on a hexagon (hence, with an hexagon on top, also facing the STM tip), the MO will appear as three-leaved clover-like features, since the tip will'see' the three pentagons on the side of the hexagon. Adsorption on a dimer separating two hexagons (we will call this a 6 : 6 dimer) will exhibit two twin bumps, and then, on a pentagon, just a single protrusion.

STM images revealed that, on different metals, C_{60} can exhibit different apparent heights (AH), and bright and dim molecules can coexist [15, 18, 30, 32, 34, 37–40] This bright and dim contrast is not due to the molecules adsorbed on different layers, as one could think at first sight. The origin of such features has been debated for the past few years but the scientific community is more and more keen to justify the difference in AH as caused by a surface reconstruction on the metal (such as a vacancy formation) which causes some molecules to 'sink' with respect to others.

Although induced formation of atomic vacancies is nowadays widely accepted and several authors have confirmed it, there is still a lot of controversy about the conditions for the formation of the vacancy and very little understanding of the mechanism driving the process. Felici *et al* reported that the temperature of formation of the vacancy is about 420 K [4], and they have shown that the fullerene/Pt interface already reconstructs at this temperature. In this sense, Shi *et al* [6] suggested that the vacancy forms above 500 K. Liu *et al* [5] showed that at RT the molecules have five different orientations, while, upon annealing to about 700 K, all of the fullerenes rotate to sit on a hexagon oriented in the same direction with respect to the Pt crystallographic directions.

There is an additional problem in understanding these complex systems. Most of the experimental results performed until now have been obtained on a particular surface structure, which is attained after specific (and sometimes bizarre) preparation conditions. This is a drawback when the kinetics of the formation plays an important role, as seems to be the case in this system. Fullerenes on Pt(111) exhibit two long range ordered superstructures, $(\sqrt{13}\times\sqrt{13})$R13.9° and $(2\sqrt{3}\times 2\sqrt{3})$R30° [4–6]. The latter is only observed after particular annealing conditions. The experimental recipe for preparing the superstructures is very delicate in the sense that small variation of the experimental conditions can give rise to the formation of different structures. All the controversies mentioned above can be regarded as uncertain terms, originated because the experimental protocol for growing the layers is not unique.

The aim of this work is to view the problem as a whole, trying to gain insight into the mechanism of vacancy formation and looking at the kinetics of the process by using a multi-technique experimental approach combined with density functional theory (DFT) calculations. We address the problem of the single-atom vacancy formation by systematically studying samples annealed at different temperatures by STM and by x-ray photoelectrons spectroscopy (XPS); this gives us information about bonding and charge transfer processes occurring upon annealing. We find the as-deposited molecules to interact weakly with the surface. This interaction increases as the surface is annealed, and the system evolves, towards a chemisorption state in which the vacancy is formed. This structural change is signaled by a charge transfer from the surface to the molecule as revealed by the XPS measurements.

DFT calculations have helped to achieve a full understanding of the process depicted by the experimental findings. The presence of single-atom vacancies in this system has been theoretically studied by Shi *et al* [6], who performed a detailed study of the differences in the electronic properties of the system in the two possible reconstructions $(\sqrt{13}\times\sqrt{13})$R13.9° and $(2\sqrt{3}\times 2\sqrt{3})$R30° using DFT calculations with the local density approximation (LDA). Based on calculations for the $(2\sqrt{3}\times 2\sqrt{3})$R30° case and the theoretical analysis of the low energy electron diffraction (LEED) patterns, they confirm that a single vacancy is present in this system, as opposed to the seven-atom hole stable in the C_{60}/Cu(111) case, and that the local bonding configuration is the same for both reconstructions. Recently, Huang *et al* [7] has revisited this problem with a gradient-corrected generalized gradient approximation (GGA) functional. He assumed a hexagonal orientation for the adsorbed fullerene and studied the bonding

configuration with and without a single atom vacancy. He also considered an adatom–vacancy pair and showed that the presence of the adatom favors the stabilization of the vacancy. This interesting work is however limited by the use of a very thin slab with only three-metal layers (not enough to obtain good energetic values as we will show below) and the use of a 4×4 periodicity and not the real $(\sqrt{13}\times\sqrt{13})$R13.9° and $(2\sqrt{3}\times2\sqrt{3})$R30° structures.

In our work, we overcome the limitations of the previous theoretical studies and provide an extensive analysis of the adsorption of the fullerenes, considering not only the ideal Pt surfaces or the final single-atom vacancy, but also suitable candidates for the intermediate steps. We will show that this comprehensive study, which describes the kinetics of the system by STM and XPS combined with the theoretical insight provided by the calculations, can elucidate most of the experimental discrepancies mentioned above and lead to a global understanding of the mechanism of the formation of the fullerene-induced vacancy.

2. Materials and methods

2.1. Experimental details

C_{60} molecules (Sigma-Aldrich, 99.9% purity) were evaporated at a rate of 0.1 monolayers (ML)/min on a clean Pt(111) sample from a Ta crucible whose temperature was monitored with a Chromel-Alumel thermocouple. The substrate was kept at RT during the evaporation. The temperature of the sample was calibrated successively either with a Chromel-Alumel thermocouple or with an infrared pyrometer or with a combination of the two.

The sample was characterized with ultra high vacuum (UHV) RT- and low temperature-STM in the ESISNA group at the Material Science Institute of Madrid in Spain, and in the M2N group of the Technical University of Eindhoven, in The Netherlands, respectively. LEED-intensity voltage (LEED-IV) curve measurement was also carried out within the ESISNA group (data not shown). High resolution XPS was measured at the SuperESCA beamline of the ELETTRA synchrotron (Trieste, Italy). This beamline has an energy resolution $E/\Delta E\sim10^4$, so even the slightest changes in the electronic configuration of the analyzed system can be recorded.

Temperature programmed desorption (TPD) was carried out at the Institute of Solid State Physics, Graz University of Technology (Austria). This UHV chamber [41] with a background pressure of about 1×10^{-10} mbar is equipped with a Pfeiffer Prisma quadrupole mass spectrometer that is used for thermal desorption measurements in line of sight. It was previously determined that the detected gases stem directly from the sample surface. Additionally, to make sure that the H_2 does not stem from other sources in the chamber a control experiment out of line of sight was made. Tantalum wires are spot welded to the back of the Pt(111) sample and used for resistive heating of the sample. The temperature of the sample is measured using a Chromel-Alumel thermocouple spot welded to the back of the crystal. The TPD measurements were made with a heating rate of 1 K s^{-1}.

Due to the large number of laboratories in which experiments were carried out, the error in measuring the temperature of the sample was unfortunately high (about 40 K). We tried to keep it as low as possible, by using when possible the combination of Chromel-Alumel thermocouples with infra-red pyrometers.

2.2. Theoretical details

Our first-principles calculations are based on DFT and employ a plane wave basis set. They have been performed with the Vienna *ab initio* simulation package (VASP) [42]. The interaction between the ions and valence electrons is described by the projector-augmented-wave method [43]. Valence band wave functions are expanded using a cutoff of 400 eV. The Brillouin zone of the $(\sqrt{13}\times\sqrt{13})$R13.9° reconstruction has been sampled with a $4\times4\times1$ Monkhorst-Pack k-point grid. No significant differences are found when using a finer $8\times8\times1$ grid.

The GGA functional proposed by Perdew, Burke and Ernzernhof [44], has been used for the description of exchange-correlation energy. We have also calculated some of the structures using the LDA, in order to compare our results with the calculations available in the literature. As discussed in section 4, LDA calculations result in stronger molecule-substrate interactions but they reflect the same general trends regarding the favorable molecular orientation and the vacancy formation found with the GGA approximation.

For the initial exploration of the potential energy surface for fullerene adsorption we have employed OpenMX [45], a very efficient DFT code based on a local orbital basis. In OpenMX, the wavefunctions are expanded as a linear combination of strictly localized pseudoatomic orbitals centered on atomic sites [46]. In these calculations we use a double-zeta basis for H and Pt and a more complete data set with two s and three p orbitals for C. The rest of the technical details are identical to the ones used in the study of the adsorption of planar PAH on Pt [47].

The surfaces are described by six-layer thick slabs, where we keep the two bottom layers fixed at the corresponding bulk positions during the structural relaxation. We use the theoretical bulk lattice constants that we have calculated for Pt with both the GGA (3.994 Å) and LDA (3.907 Å) functionals. The molecule is adsorbed on one side of the slab. A vacuum of 24 Å in the surface normal direction is used in our supercell approach. All the atoms on the molecule and the top four layers of the slab are allowed to relax until differences in the total energy per atom are below 10^{-6} eV and forces are smaller than 0.01 eV $Å^{-1}$.

We have checked that thinner slabs with three and four layers (where we allow the top two layers to relax) do reproduce the trends in energy differences between different sites but not the absolute adsorption energies. The error with the three-layer slab is around 30% and it drops to 5% with the four-layer slab. The structures, however, converge rather well

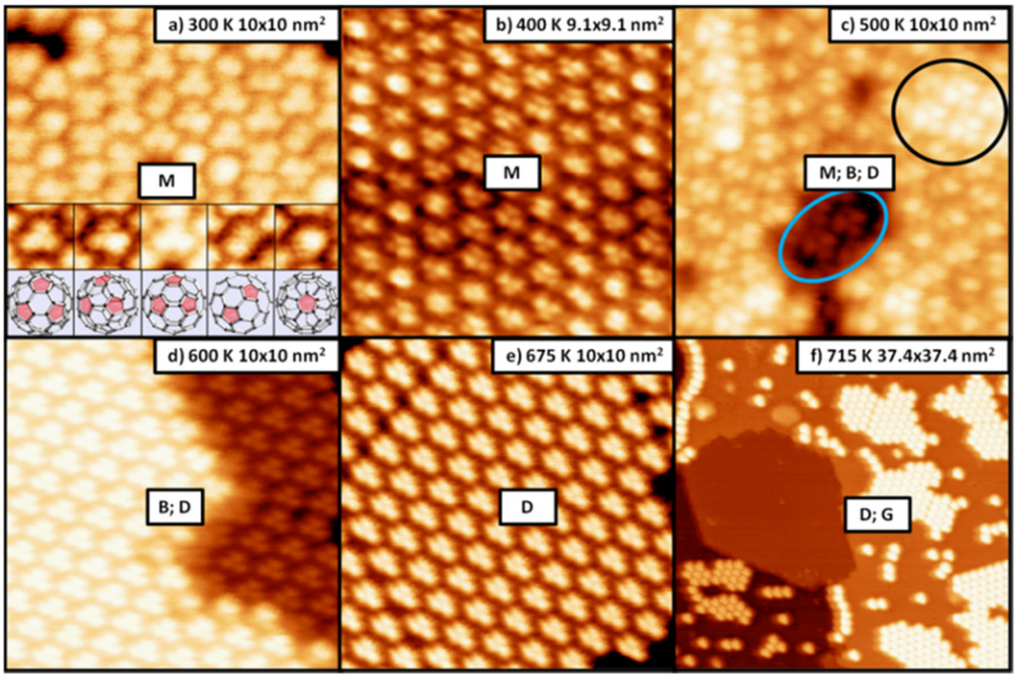

Figure 1. Series of STM images of C_{60}/Pt(111) deposited at RT and subsequently annealed to different temperatures. The annealing temperature and the size of the image are shown in the caption of the figure. M, B and D stand for medium height, bright and dim molecule, respectively. The voltage applied to the sample is $V_s = +2$ V in all the images. The inset in (a) shows the five different orientations of the molecules with the corresponding orbitals. The blue oval in (c) shows two D molecules and the black circle three B molecules. A graphene island (G) is observed in (f).

with these thinner slabs: differences in atomic positions between the calculations with four and six layers are smaller than 0.02 Å.

3. Results and discussion

3.1. STM study

Figure 1 shows STM images recorded after depositing about 0.4 ML of C_{60} molecules on Pt(111) at RT and annealing the resulting organic layer in steps to different temperatures, up to 715 K. In these images the MO of the C_{60} molecules are clearly distinguishable. After RT deposition, all the C_{60} molecules exhibit the same AH, about 6.6 ± 0.3 Å, and the fullerenes are oriented in five different configurations, as previously reported [5] and indicated in the inset of figure 1(a). The molecules are either sitting on a pentagon, on a hexagon, on a 6 : 6 dimer, or in two intermediate configurations. This type of molecules adsorbed at RT sitting on different configurations and with an AH of 6.6 Å, will be referred to, from now on, as medium-height (M) molecules. They present a $(\sqrt{13} \times \sqrt{13})$R13.9° translational symmetry but the rotational order of the individual molecules is lost. The high diffusion of these molecules on the surface and the loss of rotational order suggest that M molecules are in a physisorbed state, as it will be discussed later.

Upon slight annealing to 400 K, the molecular geometry is not altered (figure 1(b)). However, above 500 K (figure 1(c)) the topography changes drastically: molecules showing higher and lower AH's coexist with M-type molecules. All those brighter (B) and dimmer (D) fullerenes exhibit a three-leaved clover shape which indicates that they are all sitting on a hexagon with the same orientation with respect to the Pt(111) lattice. They exhibit an AH of 7.5 ± 0.3 Å and 4.8 ± 0.5 Å, respectively. These height differences are reliable and, as it will be discussed later, are based on a statistical description.

Progressive annealing of the system leads to the subsequent loss of M-type molecules and the increase of the B and D units. At 600 K (figure 1(d)) only B and D molecules are present on the sample. If we keep on annealing, the D molecules take over since all the B molecules turn into D molecules at about 675 K (figure 1(e)), and this is true up to about 715 K. At this temperature the D molecules start to decompose into graphene (G). A trained eye will distinguish a G patch in the middle of figure 1(f) coexisting with D molecules, which is induced by fullerene decomposition. In previous STM studies [48] similar G islands were explored and the typical Moire superstructures were observed.

Summarizing the information derived from figure 1, upon annealing, fullerenes exist on the Pt surface in three different states depending on the temperature; they differ in AH and orientation with respect to the crystallographic surface directions. M molecules ($AH = 6.6 \pm 0.3$ Å), present five preferential adsorption orientations; B molecules ($AH = 7.5 \pm 0.3$ Å) all sit on a hexagon and are all orientated in the same direction. D molecules ($AH = 4.8 \pm 0.5$ Å) are also sitting on a hexagon and all orientated in the same direction as B.

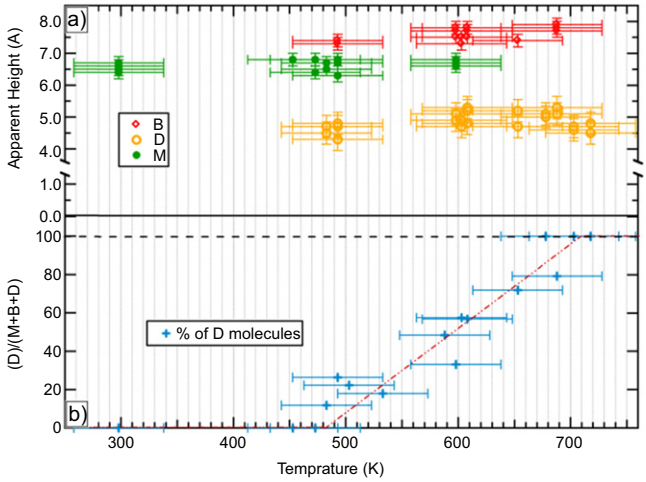

Figure 2. Apparent height and percentage of every type of fullerene on the Pt(111) surface. (a) Statistical graph of the apparent height of the molecules as a function of the temperature. It is clear that there are three types of molecules, green solid dots M (exits from RT to 590 K), red empty rhombs B (from 480 to 680 K) and yellow empty dots D (from 480 K to the decomposition temperature). (b) Percentage of D molecules (blue crosses) with respect to the total number of molecules as a function of annealing temperature. It varies linearly with temperature from 0% to 100%.

These observations can be turned quantitative with a systematic study of the relative abundance of these different fullerenes as a function of the temperature. To this goal, we have analyzed hundreds of molecules from many different STM images in order to have good statistics. Figure 2(a) shows the apparent height dispersion of the molecules in terms of the temperature of annealing (error-bars correspond to the standard deviation of about a hundred different measurements). It clearly shows the existence of the three types of molecules (M, B and D) mentioned above. Figure 2(b) represents the relative abundance of D molecules with respect to the total number of (M + B + D) molecules, as a function of the temperature. It shows statistically that the percentage of D molecules increases linearly with temperature, from 0% at RT to a total of 100% at about 700 ± 40 K.

Moreover this graph shows that the transformation is a slow process, as different types of molecules coexist in a large temperature range, indicating that the transformation cannot be considered as a first-order phase transition. For example, even if the B and D molecules appear about 490 ± 40 K, the M height molecules disappear at about 590 ± 40 K, so the M, B and D molecules are coexisting for more than 100 K. These data suggest a temperature induced molecular transformation. A molecule deposited at RT is weakly adsorbed in an M state, but as the temperature increases it will be transformed into D passing through a metastable B state, as schematically shown in figure 3.

3.2. Temperature programmed- and high resolution- XPS

In order to get insight into the nature of chemical interaction between the fullerenes and the substrate, we have measured temperature programmed XPS. The result is shown in figure 4. This image shows the changes in the intensity of the carbon 1s peak of the system in terms of binding energy (bottom axis) and the temperature (left axis). The rate of increase of the temperature in this experiment was 1 K s^{-1}. On the right-hand side we have represented what is occurring in the sample as observed by the STM images at the same temperature as the *y*-axis in the plot.

The most noticeable feature is a clear −0.15 eV shift towards lower binding energy which occurs at about 460 K. Remarkably, this shift occurs at the same temperature at which B and D molecules start appearing on the surface. A shift in a XPS core-level peak can be caused by several factors. In our case, relaxation effects are not expected to play a major role and, to a first approximation, the rigid shift of the C1s peak can be assigned to charge transfer processes. The direction of the energy shift indicates a charge transfer from Pt to C_{60}, as also predicted in [6]. The absolute value for the charge transfer derived from XPS cannot be determined precisely [49], but can be estimated to be very small, lower than 0.1 electron per molecule.

If we continue annealing beyond 650 K, the charge accumulation at the molecules is partially returned back to the surface and then the peak stretches up to show the typical peak of graphene [50] above 800 K. Photoelectron diffraction effects accounts for the final enhancement of intensity at elevated temperature.

Figure 5 shows high-resolution XPS C1s peaks of C_{60}/Pt (111) recorded at the most important temperatures and the corresponding STM image. At RT, the main peak corresponding to the sp^2 carbon forming the hexagons and the pentagons of the molecules rises at 284.05 eV, and a second peak at higher binding energy follows at 284.46 eV. The presence of the higher binding energy peak at about 0.4 eV from the main one has been observed on different surfaces such as Cu(111) [51, 52], Ag(110) [53], Au(110) [54] and others [8], and most authors relate it to an asymmetry of the main peak due to non-equivalent carbon sites or to non-uniform distribution of valence electron charge due to hybridization/chemisorption effects. A tiny shake-up feature emerges in the spectrum recorded at RT at 285.86 eV, about 1.81 eV higher than the main peak: this value is very similar to the one found by Swami *et al* [10] on the same system (shifted by 1.9 eV). Notice that the shake-up peak only exists at RT: according to Pedio *et al* [8], the satellite washes out because there is an increase in the bonding interaction with the surface, corresponding to a more covalent bond.

As discussed above, upon annealing both components shift towards lower binding energy; also, the high-energy component becomes more important. Interestingly, the spectra at 600 K and 800 K, show a very similar lineshape, indicating that both B and D molecules (one predominant at 600 K, and the other at 800 K) should present a very similar chemical bonding with the surface.

3.3. Theoretical calculations

In order to understand the experimental results discussed so far and, in particular, to provide a full picture of the fullerene

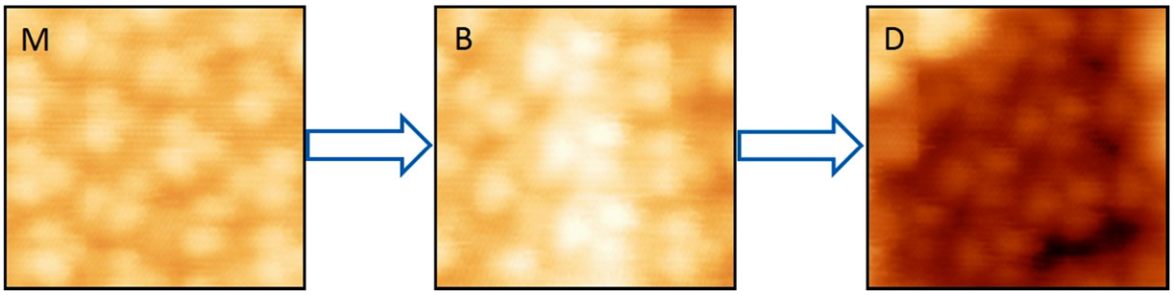

Figure 3. Schematic representation of the transition from the medium-height (M) phase to the bright (B) phase and finally, to the dim (D) phase (3.2×3.2 nm^2; sample voltage = +2.0 V).

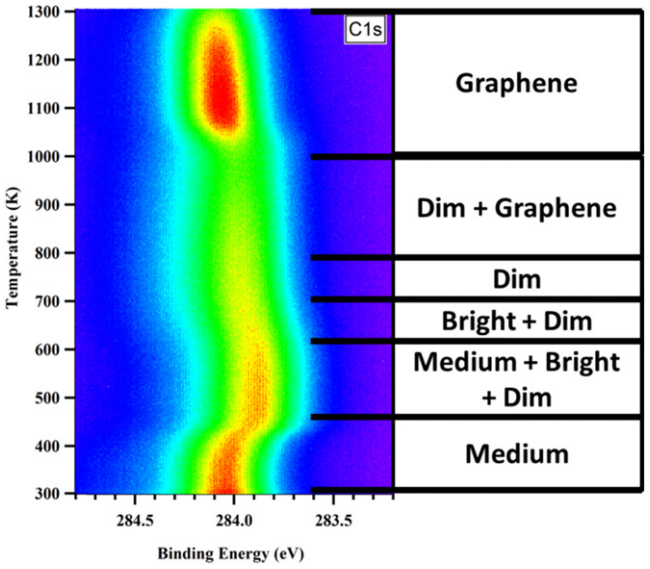

Figure 4. Real-time XPS of C1s peak of C60/Pt(111) upon annealing. The bottom axis shows the changes in binding energy, the *y*-axis shows the temperature changes. On the right, a comparison with the apparent height recorded with the STM images is given. The red in the color code indicates the highest intensity, while blue indicates the lowest intensity.

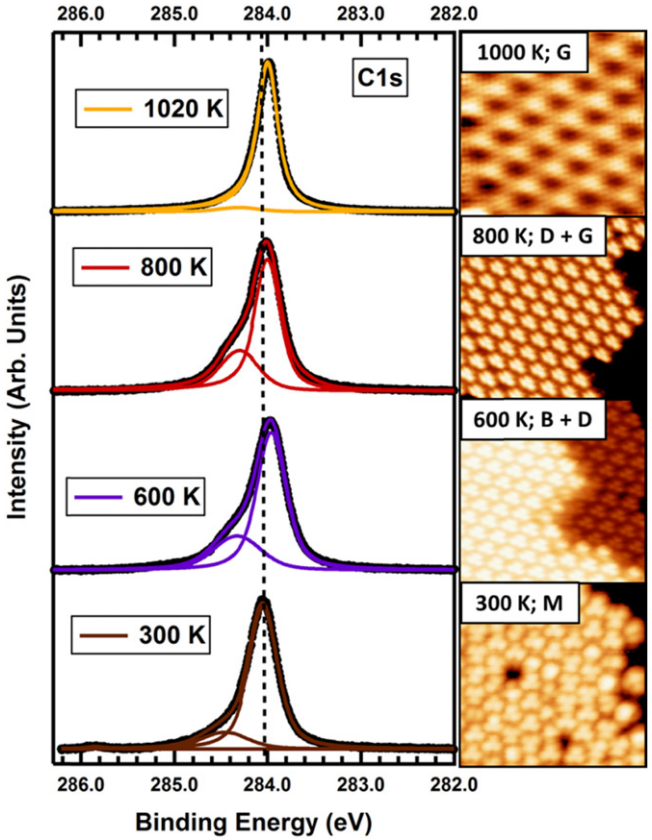

Figure 5. C1s XPS peak of C60/Pt(111) at various temperatures decomposed in curve-components, together with the corresponding STM image. All the STM images' sizes are 10×10 nm^2 and sample voltage between 2.0 and 2.5 V, except the graphene one (7×7 nm^2; $V_s = 0.15$ V). All the XPS exhibit one main peak and a smaller one at higher binding energy.

adsorption and vacancy formation mechanism, we have performed an extensive set of DFT simulations for the C_{60} molecule adsorbed on three different surfaces with a $(\sqrt{13} \times \sqrt{13})$R13.9° periodicity: an ideal Pt(111) surface, a surface with a Pt vacancy per unit cell, and on a H-covered Pt (111) surface. These calculations allow us to characterize the nature of the adsorption state (chemisorption versus physisorption), the most favorable adsorption site, and the fullerene orientation in each of these three systems. Furthermore, our results provide insight into the intermediate steps involved in the creation of Pt surface vacancies and the formation of the ordered fullerene-vacancy periodic structure.

3.3.1. C_{60} adsorption on the clean Pt(111) surface. The phase space for the adsorption of the C_{60} molecule is very complex as we have to consider many possible orientations of the molecule and different adsorption sites. To restrict their number, only those configurations that maximize the number of C–Pt bonds prior to any relaxation are considered. According to this restriction, two orientations are particularly favorable, namely with the molecule sitting either on a 6 : 6 dimer (the one separating two hexagons) or on a hexagon. For these two configurations, the possible relative atomic positions between the molecule and the substrate have also been restricted to those providing the highest number of C–Pt bonds prior to any relaxation. For the molecule sitting on a hexagon, we explored all the possible rotations of the hexagon at the bottom between 0° and 30° with respect to the [1–10] Pt crystallographic direction (0° corresponds to a perfect alignment between that hexagon and the underlying Pt hexagonal structure). For the molecule

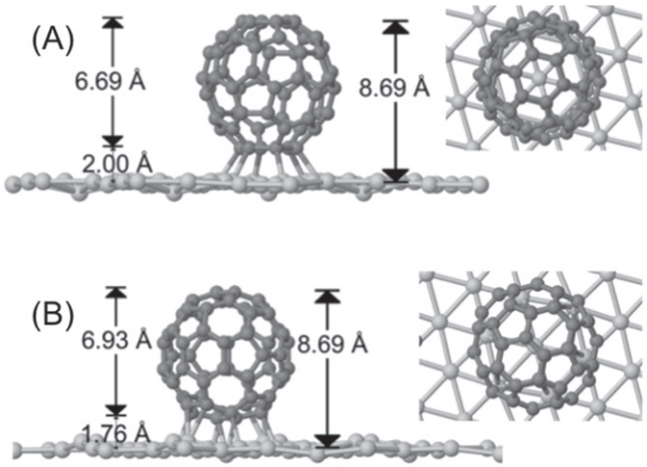

Figure 6. C60 on the pristine Pt(111)-($\sqrt{13}\times\sqrt{13}$)R13.9° surface: adsorption on (A) the hex0 and (B) the dimer30 configurations. Both side and top views of the structures are displayed. Only one substrate layer is sketched to ease the visualization.

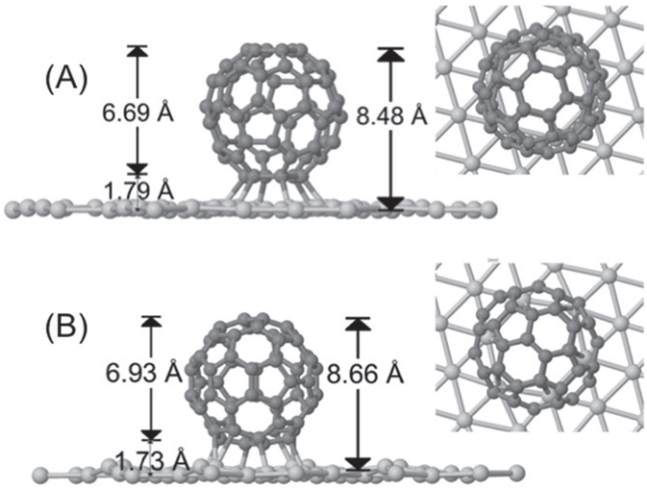

Figure 7. C60 on the Pt(111)-($\sqrt{13}\times\sqrt{13}$)R13.9° surface with a Pt surface vacancy per unit cell: adsorption on (A) the hex0 and (B) the dimer30 configurations. Both side and top views of the structures are sketched. Only one substrate layer is included to ease the visualization.

sitting on a dimer, the orientations considered follow a previous study of the adsorption of benzene and naphthalene on Pt(111) [55].

Even with the above-mentioned restrictions, the exploration of the potential energy surface around the two different geometries and all relative orientations is still a heavy task from the computational point of view. For these calculations we have employed OpenMX [45], a very efficient DFT code based on a local orbital basis. In this way, we have identified the two lowest energy configurations which will be referred to as dimer30 and hex0. They correspond to (i) the molecule sitting on a 6 : 6 dimer bridging between two Pt-hexagons at 30° with respect to the [1–10] surface direction for dimer30, and to (ii) the fullerene oriented on a carbon hexagon on top of a Pt hexagon on the surface for hex0 (see figure 6). These two configurations have been recalculated with VASP and they provide the basis for the rest of our theoretical study.

Our calculations show that the most stable configuration on the Pt(111) surface without vacancies is actually the dimer30 one, which has not been considered before in the literature. The E_{ads}, calculated as the difference between the total energy of adsorbed fullerene and the sum of the Pt slab and of the isolated fullerene, are −1.67 eV per molecule for the dimer30 and −1.50 eV for the hex0 configuration. Calculations for these two structures with the LDA approximation to the exchange-correlation functional reproduce the relative stability but overestimate the binding energies (−4.41 eV for dimer30 and −4.00 eV for hex0).

The corresponding adsorption geometries for both the dimer30 and the hex0 configurations, with an estimation of the vertical size of the fullerene and its height above the substrate are shown in figure 6. The height of the fullerene above the substrate is calculated as the average height of the dimer/hexagon atoms depending on the final adsorption orientation. The vertical size of the molecule is the difference in height between the upper and lower parts of the molecule, calculated as the average of the 'z' component of the corresponding two (six) C atoms for the dimer30 (hex0) adsorption orientation. For an isolated C_{60} molecule, the hexagon–hexagon and dimer–dimer distances are 6.50 Å and 6.95 Å respectively. While the molecule is not deformed significantly on the dimer30 configuration (dimer–dimer 6.93 Å, see figure 6), it is slightly elongated (by 0.19 Å) in the hex0 geometry.

Notice that the fullerene adsorption in both configurations induces a large corrugation on the Pt surface. In the hex0 case, the Pt atom right beneath the fullerene moves 0.42 Å downwards, while each of the six Pt atoms bonded to the fullerene are displaced upwards by 0.17 Å. For the dimer30 configuration, the changes in height with respect to the surface positions are even larger, with a −0.23 Å variation for the Pt atom below the dimer, and an upward displacements of 0.10 Å and 0.45 Å for the Pt atoms bonded to 1 and 2 carbon atoms, respectively.

3.3.2. Vacancy formation. We now address the creation of Pt surface vacancies and the formation of the ordered fullerene-vacancy periodic structure from a theoretical point of view. Motivated by the structures proposed in the literature, we start with the analysis of the stability of the dimer30 and hex0 structures upon the removal of the Pt surface atom closest to the fullerene. The atomic relaxation to the new ground state for both configurations (labeled dimer30-vac and hex0-vac) is far from trivial as the system gets trapped in local energy minima, confirming the presence of significant energy barriers to obtain the final configurations shown in figure 7. The adsorption energies, taking the Pt slab with the vacancy as the reference, are now −2.38 eV per fullerene molecule for the dimer30-vac configuration and −3.47 eV for the hex0-vac structure. Thus, in the presence of the vacancy, the hexagonal orientation is the most stable structure. The energy gain of almost 2 eV with respect to the ideal surface for hex0-vac (compared to just 0.71 eV for the dimer30-vac case) is related

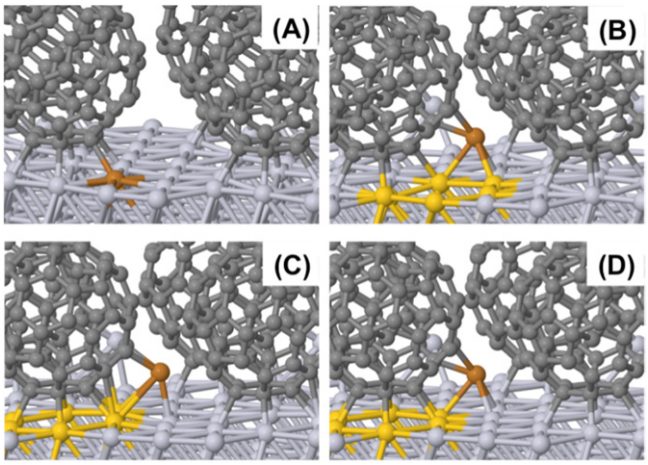

Figure 8. Relaxed structures for adatom–vacancy pairs created on the C60/Pt(111)-($\sqrt{13}\times\sqrt{13}$)R13.9° with an hex0 configuration:(A) A Pt atom (marked brown) bonded to the fullerene has been removed from the surface (B), creating a vacancy on the side of the C_{60} molecule (atoms surrounding the vacancy are highlighted in yellow), and positioned as an adatom on the neighboring hcp-site. (C) and (D) correspond to configurations where the Pt atom right below the C_{60} has been removed and positioned originally as an adatom on an fcc (C) or an hcp site (D), creating a vacancy below the fullerene.

to the release of the large strain created on the Pt substrate by the adsorption of the fullerene, resulting in an almost flat surface around the fullerene and a smaller molecule-surface distance. Calculations with the LDA approximation show the same trend, favoring the hex0-vac configuration (−6.45 eV) versus the dimer30-vac structure (−5.32). Notice that the energy difference between the two configurations in LDA (1.13 eV) is quite close to the GGA value (1.09 eV), although the absolute energies are again overestimated.

A detailed inspection of figures 6 and 7 indicates that the main effect of the vacancy in the structure is a very small reduction of the adsorption distance between the molecule and the surface of about 0.03 Å for dimer30 and 0.21 Å for hex0. In the absence of significant electronic effects, this small change in height would be indiscernible in an STM image.

The next relevant matter to investigate is the mechanism of formation of the Pt vacancies. Reference [7] suggested that the Pt atom right below the fullerene could directly migrate to the surface and form an adatom–vacancy pair. The bulk self-diffusion of a Pt atom is a costly process in terms of energy. The large strain in the Pt structure created by the fullerene adsorption is going to make this process even more difficult. Instead, we propose a two-step process in which, firstly, a Pt vacancy is created next to the fullerene, and, secondly, this vacancy migrates from the side to the position right below the molecule.

The top panel in figure 8 illustrates the creation of one of these adatom–vacancy pairs. Starting from the hex0 configuration (figure 8(A)), a Pt atom has been removed from the surface and positioned as an adatom on the neighboring hcp site, creating a vacancy aside of the C_{60} molecule (figure 8(B)). The energy cost, estimated as the energy difference between the hex0 configuration and this adatom–vacancy structure after full relaxation, is 1.50 eV. This value is significant lower than the 2.28 eV required to create this adatom–vacancy pair on the bare Pt(111) surface represented by the same four-layer slab. Therefore, the presence of the fullerene molecule eases the adatom–vacancy formation due to the additional C–Pt bonds provided by the molecule. However, the final relaxed structure is very similar to the hex0 configuration. There are no significant variations in the molecule height and the position of the Pt atoms below the molecule. Thus, the creation of this Pt vacancy on the side of the molecule does not contribute to release the stress created in the Pt surface.

This is in clear contrast with the case where the adatom–vacancy pair is created such that the vacancy is located under the fullerene, as illustrated by the results of the two calculations shown in the bottom panel of figures 8((C) and (D)). The Pt atom right below the C_{60} has been removed, creating a vacancy right below the fullerene, and has been positioned as an adatom on a neighboring fcc or hcp site. In both cases the molecule height and the release of the surface strain are almost identical to the ones achieved in the hex0-vac configuration. Notice that, in the case of the fcc adatom, the reduction of the molecule height over the surface has forced the Pt adatom to move aside, weakening the three bonds with the surface Pt atoms, that have now a bond length of 2.84, 3.31 and 3.36 Å. The most stable location for the Pt adatom compatible with this adsorption configuration of the fullerene is indeed the neighboring hcp site (figure 8(D)), where we have optimal distances for the C–Pt and Pt–Pt bonds. This structure is 0.69 eV more stable than the hex0 configuration. This combination of vacancy and hcp adatom has been proposed before in [7] but the calculation was performed on a 4×4 unit cell, not on the real ($\sqrt{13}\times\sqrt{13}$) R13.9° periodicity, resulting in an energy gain of 0.32 eV. Finally, we have to stress that both the hex0-vac and the adatom–vacancy configurations are stable, so there is an energy barrier for the migration of the vacancy from the side to the position right below the fullerene in the presence of the Pt adatom.

We now focus on the vacancy migration from the side of the molecule to right below it. It is clear that the C–Pt bonds of the adatom, while favoring the creation of the adatom–vacancy pair, impose limitations on the displacements of the fullerene molecule that are necessary to reach the final stable configuration. This is clearly illustrated by the process shown in figure 9, where the Pt adatom has been removed and the vacancy relaxes without energy barrier to the final hex0-vac configuration. These results support the idea that the formation of the ordered C_{60}-vacancy structure is indeed a two-step process. In the first step the presence of the fullerene lowers the energy cost of creating an adatom–vacancy pair on the side of the molecule. Then, after an extra annealing at higher temperature, these adatoms can be detached from the fullerenes side, removing the constraints on its relaxation, and leading to the migration of the vacancy below the fullerene without energy barrier [34].

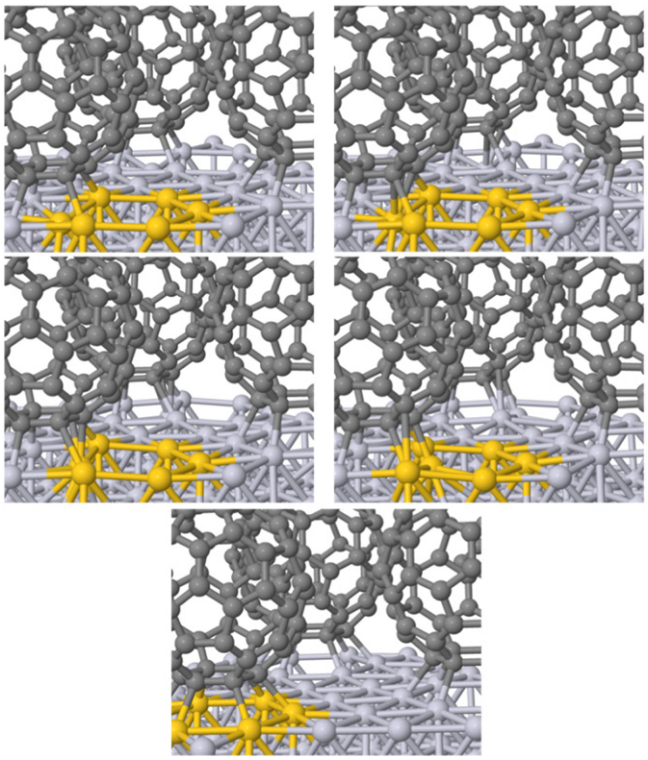

Figure 9. Snapshots for the vacancy migration from the side to the bottom of the molecule on C60/Pt(111)-($\sqrt{13} \times \sqrt{13}$)R13.9° with an hex0 configuration. The atoms surrounding the vacancy are highlighted in yellow. Notice how the Pt atom below the fullerene moves towards the right in order to fill the empty site left by the removal of a surface Pt atom when the vacancy on the side of the molecule was created. There is no energy barrier for this process, in contrast to the situation when we have an adatom–vacancy pair.

In summary, our calculations show that, on the ideal Pt (111) surface, the preferred orientation is the one where the molecule is sitting on a dimer (our dimer30 structure) with an energy difference of 0.17 eV, while in the presence of a Pt vacancy below the fullerene, the hexagonal orientation (the hex0 structure) is 1.1 eV more stable, in excellent agreement with the experiments. The driving force for the creation of the Pt vacancy is the release of the significant surface stress created by the adsorption of the molecule. Our results suggest that the formation of this vacancy is a two-step process, involving first the formation of an adatom–vacancy pair, and, then, the migration of the vacancy from the side to the position right below the fullerene.

4. Discussion

We are now in the position to combine the experimental and theoretical results presented above, to understand the nature of M, B and D molecules.

4.1. Nature of the M molecules

The first question to address is the nature of the M molecules, observed upon deposition of the fullerenes at RT, which

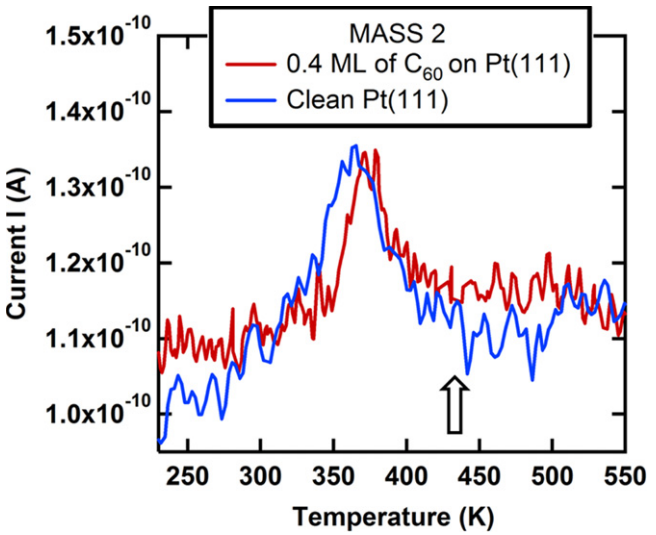

Figure 10. Temperature programmed desorption spectra of mass = 2 are shown for the case of clean Pt(111) in blue and for the case of submonolayer coverage of C_{60} on Pt(111) in red. Both cases show residual H present on the surface. The arrow indicates the threshold transformation temperature from XPS (figure 4).

completely dominate the STM images up to 490 K. The STM experiments presented above, together with evidences reported in previous works (see [5]), show that RT deposition leads to fullerenes which can diffuse until they form islands with translational symmetry, where the molecules are oriented in five different ways. These results suggest that, under these conditions, the interaction of fullerenes with the Pt(111) surface is very weak, more akin to a physisorption state than to the strong covalent chemical interaction suggested by our DFT calculations (see above) and those of other groups (see [6, 7]). All of these calculations predict that the fullerenes will bond strongly with the surface Pt atoms leading to well-fixed structures.

A possible explanation for the disagreement between the experiments and the theory could be the existence of a decoupling layer between the fullerenes and the surface. In particular, this effect may be induced by the presence of a residual submonolayer of H atoms on the Pt(111) surface. This layer would be invisible for both the STM and the XPS. At RT, these H atoms are in equilibrium with the Pt bulk and are very mobile. They can neither be visualized with the STM nor detected by XPS.

In order to confirm the existence of the 'undetectable' residual H submonolayer on a technically 'clean' Pt(111) surface, we have recorded the TPD spectra of mass 2 as shown in figure 10. This figure compares the desorption of H_2 with annealing temperature of two systems, one consisting of 0.4 ML of C_{60}/Pt(111), and the other a clean Pt surface that is taken as a reference. Surprisingly, even though the base pressure in the UHV chambers used in the experiments was better than 5×10^{-10} mbar, the desorption curves (figure 10) clearly show that there is still residual H present on the surface on both systems. Importantly, this layer desorbs completely from the surface at about 440 K, which is the same temperature (within the experimental error) at which the B

and D molecules start to appear. Albeit the total coverage of this residual H layer is very difficult to evaluate because it depends on the total residual pressure, temperature and time elapsed from the last thermal flash during the preparation protocol, we could estimate it to be around 0.15 ML. This approximation averages to more than one H atom underneath each fullerene. The existence of a residual H layer in a so-called 'clean' surface may seem unlikely, however the avidity of Pt (and other platinum group metals) for H is well known in catalysis, and this could be a kind of general process. Therefore, although this passivating layer could appear on any transition metal surface, it is more likely to appear in Pt and electronically similar metals. This H submonolayer could prevent the formation of a chemisorbed state upon deposition. Indeed, if the H is passivating the surface, the C_{60}s would not be able to bind to the Pt until this H desorbs. The slight shift of the TPD peak to higher temperatures with the fullerene layer might be due to H and/or H_2 interaction with the fullerenes before desorption [56, 57]. Such shifts are common in coadsorption systems. It is important to note that although the observed shift is small, it is significant and reproducible.

We have calculated the effect of an intermediate H layer on the interaction between the fullerenes and the Pt surface. To this aim, we have considered the adsorption of the C_{60} on a Pt(111) surface with two different hydrogen coverages. The H atoms occupy all the fcc sites in the 1 ML case (13 H atoms per $(\sqrt{13}\times\sqrt{13})$R13.9° unit cell). We have also considered a coverage close to 0.5 ML, leaving 7 H atoms per unit cell.

The calculations for the two different adsorption configurations (dimer and hexagonal orientations) show that the presence of the hydrogen reduces dramatically the interaction, with binding energies for the 1 ML case (energy difference between the whole system and the sum of the isolated molecule and H-covered slab) of −0.088 eV and −0.045 eV for the dimer30 and hex0 geometries, respectively. Reduction of the hydrogen coverage to ∼0.5 ML increases those binding energies by less than 3%. In all the cases the molecules essentially float over the surface at a distance larger than 3.15 Å and their internal structure is identical to that of the isolated molecule. vdW interactions, not included in our calculation, are not expected to modify significantly the interaction strength or the adsorption geometry. With absolute energies in the 50–90 meV range, and energy differences of 40 meV among the different adsorption configurations, we expect energy barriers that can be easily overcome by the available thermal energy, making all the orientations accessible. The weak interaction between C_{60} and H/Pt(111) has also been confirmed experimentally by H He *et al* [58]. In this work, the authors characterized the interaction of fullerenes on a pure Pt(111) surface, i.e. without H, and after passivating it with different species (H, O and a graphite adlayer). They found that the interaction is lower in the case of fullerenes on the passivated surfaces, especially in the case of the graphite adlayer. Thus, both STM experiments, TPD measurements and theory provide a strong evidence of the presence of H on the Pt(111) surface and its role in passivating the surface, leading to a physisorbed state.

4.2. Nature of the chemisorbed states: the D molecules

For annealing temperatures greater than 490 ± 40 K the fullerenes evolve into a chemisorbed state. Our STM images show: (1) the appearance of the B and D molecules, which coexist up to an annealing temperature close to 700 K; (2) all the B and D molecules are sitting on a hexagon oriented on the atomic packing surface direction (called hex0); (3) B molecules progressively transform into D as the temperature is increased; (4) a single molecular configuration (D) dominates above 700 K.

In the STM study of [5] two different regimes were also identified as the annealing temperature was increased above 500 K. At this point all the molecules rotate to sit on a hexagon. The dominance of a particular molecular orientation confirms the strong surface-adsorbate interaction predicted by the theory. Our calculations show that the presence of Pt vacancies makes the hexagonal orientation (the hex0 structure) the most stable configuration, in excellent agreement with the experiments (see figure 1). Moreover, TPD results show that beyond 440 ± 40 K (within the error of the temperature at which B and D start to appear) the H layer which passivates the Pt has left the surface, and, thus, we should assume that B molecules are also in direct contact with the surface and correspond to a chemisorbed state.

Thus, it seems clear that D molecules, the ones that prevail at high temperatures, are the most stable, and therefore, correspond to fullerenes sitting on top of a Pt vacancy as first proposed by Felici *et al* [4] based on XRD measurements, and supported by STM and LEED experiments in ref. [6].

4.3. Nature of the metastable B molecules

In the discussion above, we have clearly identified the nature of the M and D molecules as a H-decoupled physisorbed state and on-vacancy chemisorbed fullerenes, respectively. The final matter to address is the nature of the metastable intermediate state, the B state.

In light of the theoretical results discussed above, there are two possible scenarios for the formation of the B molecule. According to the TPD results, when the H leaves the surface, the molecules can interact with the Pt and rotate to sit on a hexagon either (i) without forming a vacancy, or (ii) forming an adatom–vacancy pair, in which the ejected atom remains bound to the molecule, as proposed in [7] These two models predict different vacancy formation temperatures about 600 ± 40 K for the first case (when D molecules appear) and about 440 ± 40 K for the second one.

In the first case, Pt vacancies would form upon an increase of the annealing temperature and migrate below each fullerene, progressively turning them into D molecules and forming a completely ordered fullerene-vacancy structure beyond 700 K. Our theoretical calculation would therefore imply that B molecules correspond to fullerenes in a dimer30 conformation, which would be progressively turned into D fullerenes by creating the vacancy. However, this process is not consistent with the STM experiments. Figure 1 clearly

shows that the B molecules exhibit the same three-lobe shape associated with a hexagonal orientation (hex0).

There is a second option. The fact that the B and D molecules present a similar hexagonal orientation suggests that we can correlate them with the two-step process for the formation of the ordered vacancy structure presented in the section 3.3. In this case the vacancy is created as soon as the H leaves the surface and B molecules would correspond to the intermediate step in which an adatom–vacancy pair has been created on the side of the fullerene. D molecules would form when the Pt adatoms migrate away from the C_{60} molecules, likely towards the steps (as observed for submonolayer coverage) and the vacancy would shift below the fullerene. Li *et al* have reported a similar process in which the adatom moves to the closer fullerene on Ag(111) at similar temperatures and with an energy barrier of 1.6 eV [34]

This second scenario is further supported by LEED measurements. We have recorded some LEED-IV curves for different fractional beams of the $(\sqrt{13}\times\sqrt{13})$R13.9° at different temperatures (data not shown). Above 530 K the behavior at low electron energy of the IV curves is identical, indicating that the molecular structure shall be very similar. Unfortunately, a full determination by LEED-IV was out of our capabilities. The same trend is indicated by the high resolution XPS spectra of figure 5: above 460 K the C1s core level peak for a sample with a majority of B molecules is identical to the peak of a sample with only D molecules.

Figure 4 confirms that there is a small charge transfer (~0.1 electrons per molecule) from the surface towards the molecule revealed by a C 1s core level shift of −0.15 eV that occurs around 460 K. The theory clearly reproduces this trend. Our simulations show no charge redistribution for the adsorption on the H-covered surfaces, while 0.1 electrons are accumulated on each C_{60} molecule in the chemisorbed states. This charge transfer has been determined from the subtraction of the total charge (the sum of the Bader charges on all of the fullerene atoms) in the adsorbed and the isolated molecule, and is consistent with the redistribution of the charge revealed by a plot of $\Delta\rho(\mathrm{r}) = \rho(\mathrm{r})_{\mathrm{total}} - (\rho(\mathrm{r})_{\mathrm{C60}} + \rho(\mathrm{r})_{\mathrm{slab}})$.

Thus, we believe that B molecules correspond to a metastable state in which an adatom–vacancy pair is present on the surface, and that this state has a charge redistribution associated with it. XPS experiments suggest the partial return of the surplus charge to the Pt substrate between 600–700 K, as the adatom migrates towards the step and the vacancy moves below the molecule.

5. Conclusions

STM and temperature-programmed XPS experiments conclusively show that C_{60}/Pt(111) undergoes a series of structural phase changes upon annealing. At RT, C_{60} is physisorbed on the surface, and only after annealing over 490 ± 40 K, C_{60} chemisorbs and an atomic vacancy is formed underneath each of the molecules. This evolution from a physisorbed to a chemisorbed state is associated with the presence of residual invisible H on the surface (revealed by TPD) which prevents the bonding between the fullerene and the Pt. Only when this H desorbs, the C_{60} is allowed to interact directly with the Pt, leading to the charge transfer between the two and the core level shift found in the XPS experiments

This interpretation is supported by DFT calculations that reveal the distinctive nature of the interaction in the presence of hydrogen, predict the changes in rotational order of the molecules in agreement with the experiment, and provide insight into the vacancy formation mechanism. According to these simulations, the transition between the physisorbed and chemisorbed states is not direct, as the molecules pass through a metastable state—with an Pt adatom and a surface vacancy on the side—, where there is charge excess in the C_{60}, induced by the extra bond with the ejected Pt atom. As the annealing temperature is increased, the Pt adatom diffuses away from the molecule and the extra charge is returned back to the surface, in agreement with the XPS results. This vacancy formation mechanism may be applicable to the adsorption of C_{60} on other transition and noble metal systems where the presence of adsorption-induced vacancies has been identified.

Acknowledgments

We thank the Spanish MINECO (projects MAT2011-23627, MAT2011-26534, PLE2009-0061, CSD2007-00041, CSD2010-00024) for financial support. Computer time provided by the Spanish Supercomputing Network (RES) at the Mare Nostrum III supercomputer (BSC, Barcelona, Spain) is gratefully acknowledged.

References

[1] Matsuo Y and Nakamura E 2008 Selective multiaddition of organocopper reagents to fullerenes *Chem. Rev.* **108** 3016–28
[2] Li C-Z, Yip H-L and K-Y J A 2012 Functional fullerenes for organic photovoltaics *J. Mater. Chem.* **22** 4161–77
[3] Shi X Q, van Hove M A and Zhang R Q 2012 Survey of structural and electronic properties of C_{60} on close-packed metal surfaces *J. Mater. Sci.* **47** 7341–55
[4] Felici R, Pedio M, Borgatti F, Iannotta S, Capozi M, Ciullo G and Stierle A 2005 X-ray-diffraction characterization of Pt (111) surface nanopatterning induced by C60 adsorption *Nat. Mater.* **4** 688–92
[5] Liu C, Qin Z, Chen J, Guo Q, Yu Y and Cao G 2011 Molecular orientations and interfacial structure of C60 on Pt (111) *J. Chem. Phys.* **134** 044707
[6] Shi X Q, Pang A, Man K, Zhang R Q, Minot C, Altman M and van Hove M A 2011 C60 on the Pt (111) surface: structural tuning of electronic properties *Phys. Rev.* B **84** 235406
[7] Huang M 2012 First-principles study on the reconstruction induced by the adsorption of C60 on Pt (111) *Phys. Chem. Chem. Phys.* **14** 4959–63
[8] Pedio M, Hevesi K, Zema N, Capozi M, Perfetti P, Gouttebaron R, Pireaux J J, Cadauno R and Rudolf P 1999 C60/metal surfaces: adsorption and decomposition *Surf. Sci.* **437** 249–60

[9] Giovanelli L *et al* 2003 Molecular orientation of C60 on Pt (111) determined by x-ray photoelectron diffraction *Appl. Surf. Sci.* **212-213** 57–61

[10] Swami N, He H and Koel B E 1999 Polymerization and decomposition of C60 on Pt(111) surfaces *Phys. Rev.* B **59** 8283–91

[11] Stengel M, Vita A and Baldereschi A 2003 Adatom–vacancy mechanisms for the C60/Al(111)-(6 × 6) reconstruction *Phys. Rev. Lett.* **91** 166191

[12] Maxwell A J, Brühwiler P A, Arvanitis D, Hernnäs B, Karis O, Mancini D C, Martensson N, Gray S M, Johansson M K J and Johansson L S O 1995 C60 on Al (111): covalent bonding and surface reconstruction *Phys. Rev.* B **52** R5546–9

[13] Xu G, Shi X Q, Zhang R, Pai W, Jeng H and van Hove M A 2012 Detailed low-energy electron diffraction analysis of the (4 × 4) surface structure of C60 on Cu(111): seven-atom-vacancy reconstruction *Phys. Rev.* B **86** 075419

[14] Schull G, Frederiksen T, Arnau A, Sánchez-Portal D and Berndt R 2011 Atomic-scale engineering of electrodes for single-molecule contacts *Nat. Nanotechnology* **6** 23–7

[15] Pai W W *et al* 2010 Optimal electron doping of a C60 monolayer on Cu(111) via interface reconstruction *Phys. Rev. Lett.* **104** 036103

[16] Larsson J, Elliott S, Greer J, Repp J, Meyer G and Allenspach R 2008 Orientation of individual C60 molecules adsorbed on Cu(111): low-temperature scanning tunneling microscopy and density functional calculations *Phys. Rev.* B **77** 115434

[17] Stróżecka A, Mysliveček J and Voigtländer B 2007 Scanning tunneling spectroscopy and manipulation of C60 on Cu(111) *Appl. Phys.* A **87** 475–8

[18] Pai W, Hsu C L, Lin M, Lin K and Tang T 2004 Structural relaxation of adlayers in the presence of adsorbate-induced reconstruction: C60/Cu(111) *Phys. Rev.* B **69** 125405

[19] Tang L and Guo Q 2012 Orientational ordering of the second layer of C60 molecules on Au(111) *Phys. Chem. Chem. Phys.* **14** 3323–8

[20] Tang L, Xie Y and Guo Q 2012 Probing the buried C(60)/Au (111) interface with atoms *J. Chem. Phys.* **136** 214706

[21] Tang L, Xie Y and Guo Q 2011 Complex orientational ordering of C60 molecules on Au(111) *J. Chem. Phys.* **135** 114702

[22] Britton A J, Rienzo A, O'Shea J N and Schulte K 2010 Charge transfer between the Au(111) surface and adsorbed C(60): resonant photoemission and new core-hole decay channels *J. Chem. Phys.* **133** 094705

[23] Zhang X, Tang L and Guo Q 2010 Low-temperature growth of C60 monolayers on Au (111): island orientation control with site-selective nucleation *J. Phys. Chem.* C **114** 6433–9

[24] Gardener J A, Briggs G A D and Castell M R 2009 Scanning tunneling microscopy studies of C60 monolayers on Au (111) *Phys. Rev.* B **80** 235434

[25] Schull G, Frederiksen T, Brandbyge M and Berndt R 2009 Passing current through touching molecules *Phys. Rev. Lett.* **103** 206803

[26] Schull G and Berndt R 2007 Orientationally ordered (7 × 7) superstructure of C60 on Au (111) *Phys. Rev. Lett.* **99** 226105

[27] Grobis M, Wachowiak A, Yamachika R and Crommie M F 2005 Tuning negative differential resistance in a molecular film *Appl. Phys. Lett.* **86** 204102

[28] Hinterstein M, Torrelles X, Felici R, Rius J, Huang M, Fabris S, Fuess H and Pedio M 2008 Looking underneath fullerenes on Au (110): formation of dimples in the substrate *Phys. Rev.* B **77** 153412

[29] Lu X, Grobis M, Khoo K, Louie S and Crommie M 2003 Spatially mapping the spectral density of a single C60 molecule *Phys. Rev. Lett.* **90** 096802

[30] Pai W and Hsu C L 2003 Ordering of an incommensurate molecular layer with adsorbate-induced reconstruction: C60/Ag(100) *Phys. Rev.* B **68** 121403

[31] Hsu C L and Pai W 2003 Aperiodic incommensurate phase of a C60 Monolayer on Ag (100) *Phys. Rev.* B **68** 245414

[32] Pai W, Hsu C L, Chiang C, Chang Y and Lin K 2002 Origin of peculiar STM molecular contrast in C60/Ag(100) *Surf. Sci.* **519** L605–10

[33] Cepek C, Fasel R, Sancrotti M, Greber T and Osterwalder J 2001 Coexisting inequivalent orientations of C60 on Ag (001) *Phys. Rev.* B **63** 125406

[34] Li H I *et al* 2014 Ordering and dynamical properties of superbright C60 molecules on Ag(111) *Phys. Rev.* B **89** 085428

[35] Švec M, Merino P, Dappe Y J, González C, Abad E, Jelínek P and Martín-Gago J A 2012 Van Der Waals interactions mediating the cohesion of fullerenes on graphene *Phys. Rev.* B **86** 121407

[36] Li H I *et al* 2009 Surface geometry of C60 on Ag (111) *Phys. Rev. Lett.* **103** 056101

[37] Yamada Y, Yamada S, Nakayama T, Sasaki M and Tsuru T 2011 Electronic modification of C60 monolayers via metal substrates *Japan. J. Appl. Phys.* **50** 08LB06

[38] Torrelles X, Langlais V, de Santis M, Tolentino H C N and Gauthier Y 2010 Nanoscale patterning by C60 ordering on Pt(110) *J. Phys. Chem.* C **114** 15645–52

[39] Torrelles X, Langlais V, de Santis M, Tolentino H C N and Gauthier Y 2010 Nanostructuring surfaces: deconstruction of the Pt(110)-(1 × 2) surface by C60 *Phys. Rev.* B **81** 041404

[40] Grobis M, Lu X and Crommie M 2002 Local electronic properties of a molecular monolayer: C60 on Ag (001) *Phys. Rev.* B **66** 161408

[41] Krenn G and Schennach R 2004 Adsorption and reaction of methanol on clean and oxygen modified rhodium/vanadium surface alloys *J. Chem. Phys.* **120** 5729–35

[42] Kresse G and Furthmuller J 1996 Efficient iterative schemes for *ab initio* total-energy calculations using a plane-wave basis set *Phys. Rev.* B **54** 11169–86

[43] Kresse G and Joubert D 1999 From ultrasoft pseudopotentials to the projector augmented-wave method *Phys. Rev.* B **59** 1758–75

[44] Perdew J P, Burke K and Ernzerhof M 1996 Generalized gradient approximation made simple *Phys. Rev. Lett.* **77** 3865–8

[45] OPENMX www.openmx-square.org/

[46] Ozaki T and Kino H 2005 Efficient Projector Expansion for the *Ab Initio* LCAO Method *Phys. Rev.* B **72** 045121–9

[47] Otero G, Biddau G, Ozaki T, Gómez-Lor B, Méndez J, Pérez R and Martín-Gago J A 2010 Spontaneous discrimination of polycyclic aromatic hydrocarbon (PAH) enantiomers on a metal surface *Chem. Eur. J.* **16** 13920–4

[48] Merino P, Svec M, Pinardi A L, Otero G and Martín-Gago J A 2011 Strain-driven moire superstructures of epitaxial graphene on transition metal surfaces *ACS Nano* **5** 5627–34

[49] Lüth H 2001 *Solid Surfaces, Interfaces and Thin Films* (Berlin: Springer)

[50] Otero G *et al* 2010 Ordered vacancy network 2010 induced by the growth of epitaxial graphene on Pt (111) *Phys. Rev. Lett.* **105** 216102

[51] Goldoni A *et al* 2002 C70 adsorbed on Cu (111): metallic character and molecular orientation *J. Chem. Phys.* **116** 7685–90

[52] Rowe J E, Rudolf P, Tjeng L H, Malic R A, Meigs G, Chen C T, Chen J and Plummer E W 1992 Synchrotron radiation and low energy electron diffraction studies of ultrathin C60 films deposited on Cu (100), Cu (111) and Cu (110) *Int. J. Mod. Phys.* B **6** 3909–13

[53] Magnano E, Vandré A, Cepek C, Goldoni A, Laine A, Curró G, Santaniello A and Sancrotti M 1997 Substrate-adlayer interaction at the C60/Ag(110) interface studied by high-resolution synchrotron radiation *Surf. Sci.* **379** 1066–70

[54] Maxwell A J, Brühwiler P A, Nilsson A, Martensson N and Rudolf P 1994 Photoemission, autoionization, and x-ray absorption spectroscopy of ultrathin-film C60 on Au(110) *Phys. Rev.* B **49** 10717–25

[55] Morin C, Simon D and Sautet P 2004 Trends in the chemisorption of aromatic molecules on a Pt (111) surface: benzene, naphthalene, and anthracene from first principles calculations *J. Phys. Chem.* B **108** 12084–91

[56] Krenn G, Bako I and Schennach R 2006 CO adsorption and CO and O coadsorption on Rh (111) studied by RAIRS and DFT *J. Chem. Phys.* **124** 144703

[57] Schennach R and Bechtold E 1995 Coadsorption of chlorine and carbon monoxide on a Pt (100) face *Langmuir* **11** 3815–20

[58] He H, Swami N and Koel B E 1999 Control of the growth of ordered C60 films by chemical modification of Pt(111) surfaces *Thin Solid Films* **348** 30–7